Advances in Aircraft and Spacecraft Science, *Vol. 5, No. 1 (2018) 73-105*
DOI: https://doi.org/10.12989/aas.2018.5.1.073

Constant speed, variable ascension rate, helical trajectories for airplanes

Gilles Labonté*

Department of Mathematics and Computer Science,
Royal Military College of Canada, Kingston, Ontario, Canada

(Received August 25, 2017, Revised August 28, 2017, Accepted August 29, 2017)

Abstract. A particular type of constant speed helical trajectory, with variable ascension rate, is proposed. Such trajectories are candidates of choice as motion primitives in automatic airplane trajectory planning; they can also be used by airplanes taking off or landing in limited space. The equations of motion for airplanes flying on such trajectories are exactly solvable. Their solution is presented, together with an analysis of the restrictions imposed on the geometrical parameters of the helical paths by the dynamical abilities of an airplane. The physical quantities taken into account are the airplane load factor, its lift coefficient, and the thrust its engines can produce. Formulas are provided for determining all the parameters of trajectories that would be flyable by a particular airplane, the final altitude reached, and the duration of the trajectory. It is shown how to construct speed interval tables, which would appreciably reduce the calculations to be done on board the airplane. Trajectories are characterized by their angle of inclination, their radius, and the rate of change of their inclination. Sample calculations are shown for the Cessna 182, a Silver Fox like unmanned aerial vehicle, and the F-16 Fighting Falcon.

Keywords airplane helical trajectory; automatic trajectory planning; banked turn; airplane equation of motion; helical arc connection

1. Introduction

The work reported in this article is a contribution to the enterprise of endowing unmanned aerial vehicles (UAVs) with the ability to accomplish missions without human intervention. It is concerned in particular with providing airplanes with the means to re-plan their trajectory when unforeseen circumstances require them to modify their flight plan.

An efficient approach to constructing trajectories was introduced by Frazzoli *et al.* (2005). It consists in concatenating elementary trajectory segments, called motion primitives, taken from a finite library. The most often used segments are rectilinear, circular and helical. The properties of these segments could have been determined beforehand, and stored in the memory of the airplane computing device. The main advantage of this approach lies in its minimizing of the calculations since then only the connection between the segments and a few adjustments to the motion

*Corresponding author, Emeritus Professor, E-mail: gilles.labonte@rmc.ca

http://www.techno-press.org/?journal=aas&subpage=7 ISSN: 2287-528X (Print), 2287-5271 (Online)

primitives have to be calculated. A somewhat similar, often used, approach consists in firstly building a skeleton trajectory from connected rectilinear segments, and secondly smoothing out the connections in order to keep the velocity continuous. Geometrically speaking, this smoothing can be easily done with splines. This approach is described in, among others, Judd (2001), Zheng *et al.* (2003), Nikolos *et al.* (2003) and Yang and Sukkarieh (2010). Smoothing with splines has the disadvantage of producing final trajectories that may deviate considerably from the initial stick trajectories. Furthermore, the splines are not easily analysed for their flyability by airplanes, and, to our knowledge, no such analysis has yet been performed. Another popular path smoothing method uses arcs of circles. It is more manageable in terms of determining the flyability of the trajectory. This approach was described by Chandler *et al.* (2000), Jia and Vagners (2004), Chitsaz and LaValle (2007), Hwangbo *et al.* (2007), Li Xia *et al.* (2009), Ambrosino *et al.* (2009), *Babaei and Mortazavi (2010),* Hota and Ghose (2010). It was noted that in certain situations, in which the space is restrained, helical segments would also have to be used. Such segments have been included in the elementary trajectory set by Boukraa *et al.* (2006), Chitsaz and LaValle (2007), Narayan *et al.* (2008), Tsiotras *et al.* (2011) and Beard and McLain (2015). It is sometimes possible to connect the two successive rectilinear segments of the path with a single circular arc. However, most of the time the dynamics of the airplane does not allow for such a simple connection, and the two rectilinear segments have to be connected with three or more circular arcs as mentioned in Roberge *et al.* (2012).

In the present article, we propose a new type of motion primitive that consists in a constant speed helical trajectory with varying ascension angle. It could be used advantageously to replace the above mentioned smoothing arcs in that the calculations required are much simpler. It can directly link two trajectory segments of any type, with different inclinations and directions, while keeping the velocity continuous. Fig. 1 shows an example of such a helical trajectory. In this example, the airplane arrives from below, on a rectilinear segment, inclined at an angle of 10^0. At one point, it starts flying on the helical trajectory, on which it ascends until it reaches the desired inclination angle of 25^0, direction and altitude. At this point, it leaves the helical trajectory to pursue its course on a rectilinear segment, in a different direction. A similar helical segment can, of course, be used for descending instead of ascending trajectories. In the following analysis, we consider separately ascending and descending trajectories. Trajectories in which the inclination angle changes sign would then simply be considered as a concatenation of two such trajectories, connected in a continuous fashion, with a continuous tangent. Note that circles can be considered as helix with an angle of ascension of 0^0, and straight lines, when $R \rightarrow \infty$.

Helical trajectories are also interesting by themselves. Crawford and Bowles (1975) pointed out the advantages of such trajectories, for airplanes taking off or landing in a densely populated area with respect to safety and noise reduction. Tsiotras *et al.* (2011) and Dai and Cochran (2009) also discussed helical trajectories as time optimal climbing and landing trajectories.

In most studies on trajectory planning, the airplane is modeled as a Dubins (1957) vehicle that flies at constant speed, and that has a bounded ascension rate and turning radius. Relatively few studies use more sophisticated models that include to various degrees, more realistic airplane dynamics. In the present study, we have considered the realistic airplane dynamics model described in Anderson (2000).

The flyability of inclined rectilinear trajectories, circular segments, and helical trajectories with constant ascension angle has been analyzed in Labonté (2012, 2015, 2016, 2017). Formulas for the amount of fuel, required for the longer segments of trajectory, were provided in these studies. Helical trajectories are rarely discussed in airplane dynamics manual; a few make some remarks

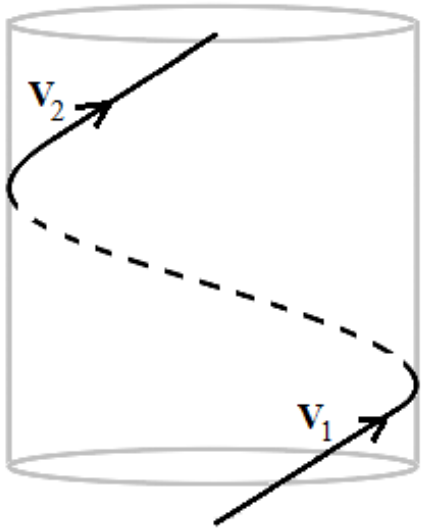

Fig. 1 Connection of two rectilinear segments of velocities $\mathbf{V}_1$ and $\mathbf{V}_2$ with a helical trajectory of varying ascension angle

about bank turns accompanied with vertical motion, such as in Section 15 of Colwley and Levy (1920), in Section 10.4 of Etkin (1972), in Section 8.2 of Mair and Birdsall (1992) and in Chapter 3 of Phillips (2004). In all these discussions of helical trajectories, the speed as well as the vertical component of the velocity are considered constant. Furthermore, all these authors, except for Colwley and Levy (1920), consider small elevation angles θ with respect to the horizontal, so that $\sin(\theta) \approx \theta$ and $\cos(\theta) \approx 1$. Goman *et al.* (2008) distinguish themselves by considering realistic equations of motion for an airplane on a constant speed, constant ascension rate, helical trajectory, which includes the rotational as well as the translational dynamics of the airplane. They examined the airplane limitations and showed how to obtain attainable equilibrium states. Since most UAVs and fighter airplanes can fly steep trajectories, for which the small ascension angle approximation is not justified, arbitrary ascension angles are considered in the present study.

1.1 Assumptions about the airplane dynamics

Cowley and Levy, in Section 15 of their book (1920) point out that a rigorous treatment of curved trajectories is extremely complicated because of the imperfectly known influences of the variations in aerodynamic forces along the wings, due to their non-symmetric role in the motion. They then mention that "any increase of drag due to the angular velocity of the aircraft and the deflections of the control surfaces can be neglected in comparison with the dominant lift-dependent drag". Von Mises in Chapter XVIII of his book (1945) confirms this statement by performing some calculations; he further makes the comment concerning bank turns: "the moments required for maintaining the steady rotation are unimportant under normal conditions". Mair and Birdsall in Chapter 8 of their book (1992) make the same comment. In the present work, we therefore also assume that, on the trajectories considered, the motion of rotation of the airplane about its center of mass does not affect appreciably the motion of its center of mass. Because the helical trajectories studied here are destined to serve as connections between other segments of

trajectory, we consider that they will not last very long, and thus, the change in mass due to fuel consumption can be neglected. This assumption is corroborated by the calculations done in Labonté (2017), of the amount of fuel required to fly on constant inclination helical trajectories that extend all the way from sea level to the service ceiling of the airplanes. As stated in this article, "The change in weight over the longest possible (helical) trajectory is rather small. For descending flight, in particular, it is always below 2.5% of the total amount of fuel. For ascending flights, it reaches up to 8.5% for the Cessna 182, 6% for the Silver Fox and 2% for the Hercules". Therefore, we can very accurately approximate the amount of fuel used by that used on a constant ascension rate helical trajectory of the same length. The amount of fuel used will be particularly small when the helical trajectory is used for connecting two other segments of trajectory. We have also neglected the perturbations of the atmosphere.

Finally, we reiterate the remark made in Chapter 3 on "Aircraft Performance" of Phillips (2004), to the effect that the material we present "should be thought of as only a preliminary study of airplane performance. In such a study, the emphasis is placed on obtaining closed-form analytic solutions suitable for preliminary design".

1.2 Organisation of the article

The first section presents the geometrical description of constant speed helical curves with varying ascension rate. The position, velocity, acceleration and radius of curvature are written in terms of Frenet-Serret coordinates. The equation of motion is then presented, and decomposed along the Frenet-Serret axes. Formulas are given for the bank angle, the load factor, the lift coefficient and for the thrust and power required for the motion on such trajectories. The constraints imposed by the limitations of these airplane parameters are derived. A condition, called "continuability condition" is stated that guarantees that the helical trajectory segment considered can be connected to rectilinear segments or can be continued as helical trajectories with constant ascension rate.

Non-descending trajectories and non-ascending trajectories are examined in turn. The possible ranges of speed, radius of the helix and ascension rate are derived from the dynamical constraints. Examples of tables of speed intervals for which trajectories are possible at specified angles of inclination are constructed, firstly for non-descending trajectories and then for non-ascending trajectories. This is done for airplanes that have similar properties as the following well known three different airplanes, the required characteristics of which are listed in Appendix A:

- the Cessna 182 Skylane, with a constant speed propeller,
- a Silver Fox like unmanned aerial vehicle (UAV) with a fixed pitch propeller,
- the F-16 Fighting Falcon which is a jet propulsed airplane.

2. Description of constant speed, variable ascension rate helical trajectories

Let us consider an airplane that flies on a vertical axis helical trajectory at the constant speed V_∞, with variable vertical component and variable rotational speed. We select the coordinate system such that the helix is centered on the z-axis, and passes through the point [R, 0, 0] at t = 0, with an angle of inclination of q_0 with respect to a horizontal plane. The position of the center of mass of the airplane is then described by

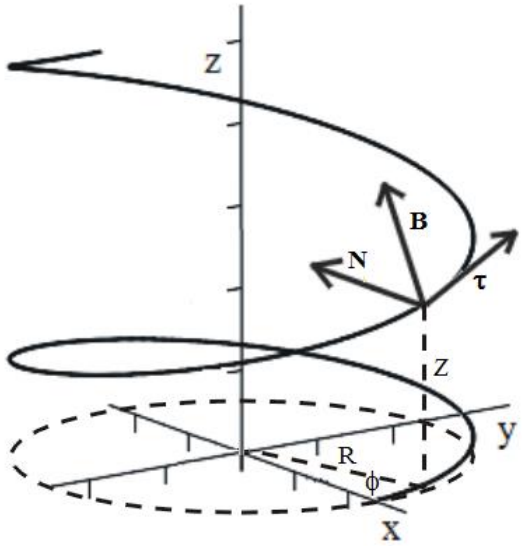

Fig. 2 Ascending helical trajectory with increasing ascension rate, showing coordinates f, R, z and the Frenet-Serret unit vectors $\boldsymbol{\tau}$, **B**, **N**

$$\mathbf{x}(t) = \left[R\cos(\phi),\, \varepsilon R\sin(\phi),\, z\right], \tag{1}$$

in which R is the constant radius of the cylinder on which the trajectory unfolds. The angle of rotation about the cylinder axis Φ and the altitude z are both time dependent. ε = +1 if the trajectory turns about the z-axis in the counterclockwise direction and ε = -1 if it turns in the counterclockwise direction. For simplicity, we shall hereafter consider e to be +1; the formulas for ε = -1 would be derived in the same manner. Fig. 2 shows such a trajectory with ε = +1, and z' > 0. The velocity is

$$\mathbf{v}(t) = \left[-R\phi'\,\sin(\phi),\, R\phi'\,\cos(\phi),\, v_z\right], \tag{2}$$

and the constant speed V_∞ is,

$$V_\infty = \sqrt{v_\phi^2 + v_z^2} \qquad \text{with} \qquad v_\phi = R\phi' \qquad \text{and} \quad v_z = z'$$

If θ is the angle of ascension of the helix, measured from an horizontal plane, then $0 \le |\theta| < \pi/2$ and

$$v_\phi = V_\infty \cos(\theta) \qquad \text{and} \qquad v_z = V_\infty \sin(\theta)$$

θ is positive when the airplane is ascending and negative when it is descending. The Frenet-Serret frame of reference $\{\boldsymbol{\tau}, \mathbf{N}, \mathbf{B}\}$ is particularly useful in the description of such trajectories. Fig. 2 shows the three-unit vectors $\boldsymbol{\tau}$, **N** and **B**. $\boldsymbol{\tau}$ is the unit tangent vector that is in the direction of the velocity

$$\boldsymbol{\tau} = \left[-\cos(\theta)\sin(\phi),\, \cos(\theta)\cos(\phi),\, \sin(\theta)\right].$$

If s denotes the distance traveled on the helix, $\frac{ds}{dt} = V_\infty$, and the arc length Δs, that is the distance traveled between times t_s and t_f is simply $\Delta s = V_\infty (t_f - t_s)$. The unit normal vector **N** is defined such that

$$\frac{d\boldsymbol{\tau}}{ds} = \mathrm{K}\mathbf{N}$$

in which K is the curvature; $R_c = 1/K$ being the radius of curvature. Thus

$$\mathrm{K} = \left\{ \left[\frac{\theta'}{V_\infty} \right]^2 + \left[\frac{\cos^2(\theta)}{R} \right]^2 \right\}^{1/2} \tag{3}$$

And $\mathbf{N} = \frac{\theta'}{\mathrm{K}V_\infty}\left[\sin(\theta)\sin(\phi), -\sin(\theta)\cos(\phi), \cos(\theta)\right] - \frac{\cos^2(\theta)}{\mathrm{K}R}\left[\cos(\phi), \sin(\phi), 0\right].$

The acceleration of the airplane on this trajectory is

$$\mathbf{a}(\mathrm{t}) = \mathbf{v}'(\mathrm{t}) = \frac{V_\infty^2}{R_c}\mathbf{N}(\mathrm{t}). \tag{4}$$

The unit binormal vector **B**, which is defined as $\boldsymbol{T} \times \mathbf{N}$, is

$$\mathbf{B} = \frac{\theta'}{\mathrm{K}V_\infty}\left[\cos(\phi), \sin(\phi), 0\right] + \frac{\cos^2(\theta)}{\mathrm{K}R}\left[\sin(\theta)\sin(\phi), -\sin(\theta)\cos(\phi), \cos(\theta)\right].$$

Note that if the trajectory turned in the clockwise direction with respect to the z-axis, **B** would be pointing downward.

3. The forces at play

The physical forces at play are

- the lift **L**,
- the gravitational force $\boldsymbol{W} = -W\boldsymbol{k}$, with $\boldsymbol{k} = [0, 0, 1]$,
- the longitudinal force that is composed of the thrust produced by the propulsion system T, and the drag D; its value being $(T - D)\boldsymbol{\tau}$.

The lift **L** is perpendicular to the velocity of the airplane and the airplane bank angle b, is measured with respect to the binormal of the trajectory. Thus, as shown in Fig. 3, **L** can be written as

$$\mathbf{L} = \mathrm{L}\cos(b)\,\mathbf{B}(\mathrm{t}) + \mathrm{L}\sin(b)\mathbf{N}(\mathrm{t}).$$

The Newton equation of motion for the airplane center of mass is

$$\frac{W}{g}\mathbf{a} = \mathbf{L} + \mathbf{W} + (T - D)\boldsymbol{\tau}. \tag{5}$$

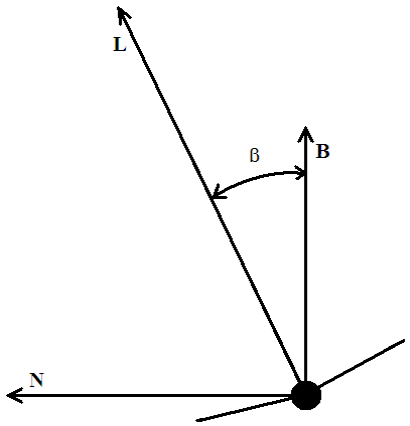

Fig. 3 The angle of bank in relation to the unit vectors **N** and **B**

The **N**, **B** and $\boldsymbol{\tau}$ components of this equation are respectively

$$L\sin(\beta) = A_c W \text{ with} \qquad A_c = \left[\frac{\mathrm{K}V_\infty^2}{g} + \frac{\theta'\cos(\theta)}{\mathrm{K}V_\infty}\right] \tag{6}$$

$$L\cos(\beta) = B_c W \qquad \text{with} \qquad B_c = \frac{\cos^3(\theta)}{\mathrm{K}\,R}, \tag{7}$$

$$T = D + W\sin(\theta). \tag{8}$$

4. A new type of varying ascension rate trajectory

Among the infinite possible ways of varying the vertical velocity on a helical trajectory, there are very few for which the equation of motion is exactly solvable. We present one that we found particularly interesting, in that it allows to manage rather easily the flyability conditions for an airplane on that trajectory. For these, the angle of inclination θ varies as

$$\theta' = k\cos(\theta) \qquad \text{where} \quad k = \frac{\lambda}{V_\infty} \quad \text{and } \lambda \text{ is a constant.} \tag{9}$$

l and k have the sign of the rate of change of the angle of ascension θ. Eq. (9) is easily integrated to yield

$$\sin(\theta) = \frac{e^{2k\tau} - C^2}{e^{2k\tau} + C^2} \qquad \text{with t = (t - t}_0\text{) and} \qquad C = \frac{\cos(\theta_0)}{1+\sin(\theta_0)}, \tag{10}$$

where t_0 is some initial instant of time, and θ_0 the value of θ at this instant. Note that C is always positive. Eq. (10) implies

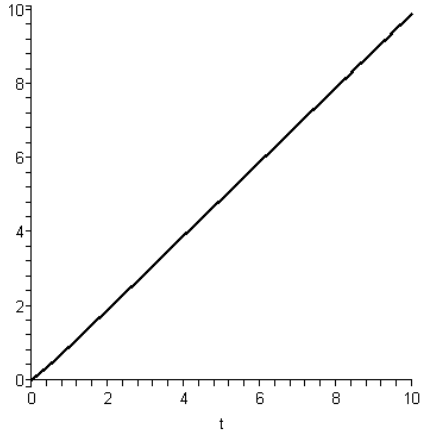

Fig. 4 Graph of h(t), with $h_0 = 0$, k = 1 and C = 9

$$\cos(\theta) = \frac{2C e^{k\tau}}{e^{2k\tau} + C^2}. \tag{11}$$

On this trajectory, the ascension angle θ_f is reached at the instant of time t_f

$$t_f = t_0 + \frac{1}{k} \ln\left\{ \frac{C(1+\sin(\theta_f))}{\cos(\theta_f)} \right\}. \tag{12}$$

4.1 Altitude

The altitude varies according to the equation

$$\frac{dh}{dt} = v_z = V_\infty \sin(\theta). \tag{13}$$

Upon integrating this equation, one obtains

$$h = h_0 + \frac{V_\infty^2}{\lambda} \{\ln\cos(\theta_0) - \ln\cos(\theta)]\}. \tag{14}$$

We remark that the variation of h with time is almost linear, as can be seen in Fig. 4, in which $h_0 = 0$, k = 1, and C = 9.

4.2 Angle of rotation φ

The tangential speed is $v_\phi = R\phi' = V_\infty \cos(\theta)$. Eq. (9) implies that

$$\phi' = \frac{V_\infty^2}{\lambda R} \theta'. \tag{15}$$

The helix is considered to be traveled in a single rotating direction; thus Φ' keeps the same sign on the trajectory. Since λ is a constant, θ' must also keep the same sign on the whole trajectory. Eq. (15) is readily integrated to yield

$$\phi = \phi_0 + \frac{V_\infty^2}{\lambda R}\left[\theta - \theta_0\right] \qquad \forall \text{ t.} \tag{16}$$

where f_0 is the angular coordinate at $t = t_0$.

4.3 Curvature

Eq. (3) for the curvature yields

$$\mathrm{K} = \cos(\theta)\left\{\frac{\lambda^2}{V_\infty^4} + \frac{\cos^2(\theta)}{R^2}\right\}^{1/2}. \tag{17}$$

5. Bank angle

Upon dividing Eq. (6) by Eq. (7), the following equation is obtained for the bank angle

$$\tan(\beta) = \frac{\mathrm{A_c}}{\mathrm{B_c}}. \tag{18}$$

The bank angle varies on the trajectory, and from Eq. (18), there follows

$$\sin(\beta) = \frac{A_c}{\sqrt{A_c^2 + B_c^2}} \qquad \cos(\beta) = \frac{B_c}{\sqrt{A_c^2 + B_c^2}}. \tag{19}$$

A straightforward calculation shows that

$$A_c^2 + B_c^2 = \left[\frac{V_\infty^2 \tilde{\mathrm{K}}}{g}\right]^2 \qquad \text{with} \qquad \tilde{\mathrm{K}} = \cos(\theta)\left\{\frac{\tilde{\lambda}^2}{V_\infty^4} + \frac{\cos^2(\theta)}{R^2}\right\}^{1/2}. \tag{20}$$

where $\tilde{\lambda} = \lambda + \mathrm{g}$.

6. Load factor

According to Eq. (2), the load factor is

$$n = \frac{L}{W} = \sqrt{A_c^2 + B_c^2}. \tag{21}$$

In order to ensure the integrity of the airplane structure, its value has to be limited such that

$$n \le n_{max},$$

Upon using Eq. (20), this bound on n can be expressed as

$$\tilde{\mathrm{K}} \le \frac{g\, n_{\max}}{V_\infty^2}. \tag{22}$$

Upon squaring each side of this inequality, one obtains

$$\cos^2(\theta)\left\{\frac{\tilde{\lambda}^2}{V_\infty^4}+\frac{\cos^2(\theta)}{R^2}\right\} \le \left[\frac{g\, n_{\max}}{V_\infty^2}\right]^2 \qquad \forall\ \theta. \tag{23}$$

This inequality holds for all values of θ if and only if it holds when its left-hand-side (LHS) is maximum, which occurs when $\cos(\theta)$ is maximum. We denote by the index "m" the smallest value of a variable and by the index "M" its largest value. Thus "$\cos_m$" and "$\cos_M$" represent respectively the smallest and the largest value that $\cos(\theta)$on the trajectory, and "$\sin_m$" and "$\sin_M$" the smallest and the largest value that $\sin(\theta)$. (23) can then be written as

$$\frac{\tilde{\lambda}^2}{V_\infty^4}+\frac{\cos_M^2}{R^2} \le \left[\frac{g\, n_{\max}}{V_\infty^2 \cos_M^2}\right]^2. \tag{24}$$

7. Lift coefficient

Upon replacing L by its expression in Eq. (6), the following expression for the lift coefficient C_L can be derived

$$C_L = \frac{2W}{\rho_\infty S V_\infty^2}\sqrt{A_c^2+B_c^2} = \frac{2W\,\tilde{\mathrm{K}}}{g\rho_\infty S}. \tag{25}$$

C_L must satisfy the constraint $C_L \le C_{L\max}$, thus

$$\tilde{\mathrm{K}} \le \alpha \qquad \text{with} \qquad \alpha = \frac{g\,\rho_\infty S C_{L\max}}{2W}. \tag{26}$$

Upon squaring each side of this inequality, there results

$$\cos^2(\theta)\left\{\frac{\tilde{\lambda}^2}{V_\infty^4}+\frac{\cos_M^2}{R^2}\right\} \le \alpha^2 \quad \forall\ \theta. \tag{27}$$

This inequality holds for all values of θ if and only if it holds when $\cos(\theta)$ is maximum. Thus

$$\frac{\tilde{\lambda}^2}{V_\infty^4}+\frac{\cos_M^2}{R^2} \le \frac{\alpha^2}{\cos_M^2}. \tag{28}$$

(23) and (28) have the same LHS; they will therefore hold if and only if their LHS is smaller or equal to the smallest of their two right-hand-sides (RHS). This can be written as a single inequality

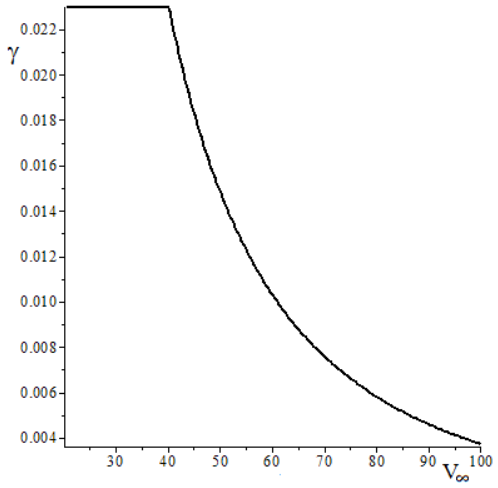

Fig. 5 Graph of $\gamma(V_\infty)$

$$\frac{\tilde{\lambda}^2}{V_\infty^4} + \frac{\cos_M^2}{R^2} \le \gamma^2(V_\infty, \cos_M), \tag{29}$$

with

$$\gamma(V_\infty, \cos_M) = \begin{cases} \dfrac{\alpha}{\cos_M} & if\ V_\infty \le V_c \\ \dfrac{g\, n_{\max}}{V_\infty^2 \cos_M} & if\ V_\infty > V_c \end{cases} \quad \text{with} \quad V_c = \sqrt{\frac{g\, n_{\max}}{\alpha}}. \tag{30}$$

Fig. 5 shows how Γ varies with V_∞, for a Cessna 182, with $\cos_M = 1$.

8. Thrust and power required

There are two constraints related to the thrust of the airplane; the first one is that it should be large enough for the airplane to be able to follow the trajectory. The second one is that it should be non-negative since a negative thrust corresponds to a deceleration of the airplane, while its speed should be constant. Upon substituting the value of the drag D and expanding the lift coefficient, according to Eqs. (25) and (20), the expression for the thrust required, given in Eq. (4), becomes

$$T_R = \overline{C}_{D0} V_\infty^2 + \frac{\Gamma V_\infty^2 \cos^2(\theta)}{g^2}\left[\frac{\tilde{\lambda}^2}{V_\infty^4} + \frac{\cos^2(\theta)}{R^2}\right] + W \sin(\theta). \tag{31}$$

in which

$$\overline{C}_{D0} = \frac{1}{2}\rho_\infty S C_{D0} \qquad \text{and} \qquad \Gamma = \frac{2W^2}{\pi e A R \rho_\infty S}. \tag{32}$$

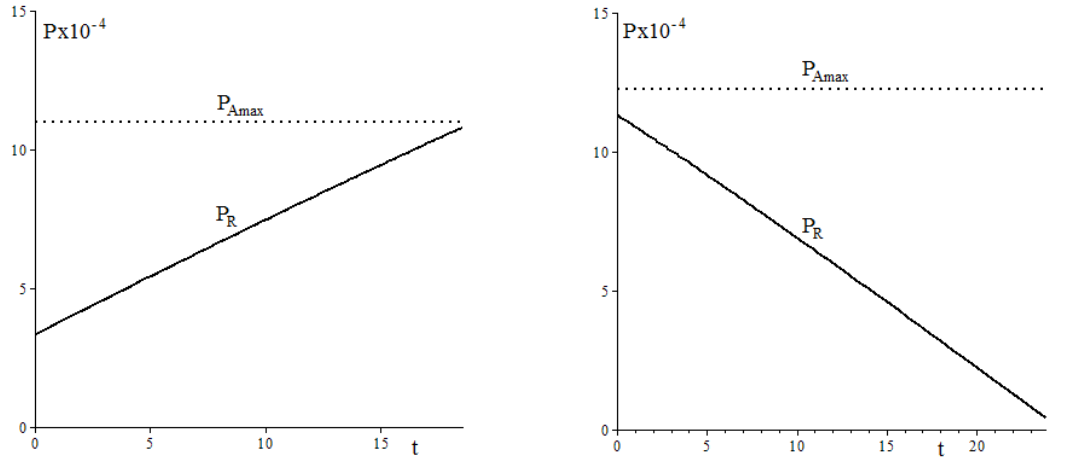

(a) Ascending trajectory with θ from 0^0 to 15^0 (b) Descending trajectory with θ from 0^0 to -15^0

Fig. 6 Power required P_R (solid line) and the maximum power available P_{Amax} (dotted line), for the Cessna 182 on an ascending trajectory in (a) and a descending trajectories in (b)

The power required for the motion is $P_R = V_\infty T_R$. The thrust is bounded above by the maximum amount that the airplane propulsion system can provide. For propeller airplanes, this bound is expressed in terms of the maximum power available P_{Amax} as

$$P_R \leq P_{Amax}(V_\infty). \tag{33}$$

The dependence of P_{Amax} on the speed is explained in Appendix A. For jet airplanes, the upper boundedness of the thrust is expressed as

$$T_R \leq T_{Amax}, \tag{34}$$

in which T_{Amax} is the maximum thrust available, which can be considered as essentially independent of the speed. Fig. 6(a) shows how the power required P_R and the power available P_{Amax} vary with time, as the Cessna 182, ascends on a helical trajectory with inclination that varies from 0^0 to 15^0, R = 150 m, V_∞ = 35 m/s, λ = 0.5 m/s^2. Note that the curves are similar when the trajectory descends while the inclination increases. Fig. 6(b) shows the same variables on a trajectory with inclination that varies from 0^0 to -15^0, R = 70 m, V_∞ = 45 m/s, λ = - 0.5 m/s^2. Again, the curves are similar when the trajectory ascends but the inclination angle decreases.

9. Continuability condition

Since l is a constant, one can see from Eqs. (10) and (11) that, as time goes to infinity, the ascension angle θ increases all the way to p/2 or decreases to $-\pi/2$. However, for most airplanes, there is a limit imposed on the magnitude of θ by their dynamical abilities; the helical trajectory can then last only for a limited interval of time. Even if an airplane could fly vertically, as a jet fighter such as the F-16, the trajectory will necessarily also be bounded between the ground and its service ceiling. Thus, in all cases, the helical trajectory can only last for a finite time, and at its end, the airplane must be able to continue its course on a different flyable trajectory. In order to

ensure this, we impose a boundary condition that we call "continuability condition". It requires that, at the end of the helical trajectory, the airplane should be in a state that allows it to keep on flying stably on another trajectory segment. We ask similarly that it arrives on the inclination varying helical trajectory in a state that corresponds to it flying on a stable trajectory segment. In practice, this means that all the constraints that are imposed on the inclination varying helical trajectory should also be satisfied at the initial and final angles θ_0 and θ_f with l set equal to 0. This is necessary and sufficient for the airplane to continue its course on a constant inclination helical, or a rectilinear or circular segments, which are, respectively, helixes with $R\to\infty$ and $\theta = 0$. This condition is required when concatenating motion primitives in trajectory planning and, it should be general enough since any flyable trajectory should behave locally as one of these trajectories. For example, this condition would require that (29) hold with $\lambda = 0$ and $\cos(\theta) = \cos_M$ and $\cos_m$; for which it is actually sufficient to have

$$\frac{\cos_M^2}{R^2} \le \gamma^2(V_\infty, \cos_M) - \frac{g^2}{V_\infty^4}. \tag{35}$$

Note that the requirement that the RHS of (35) be positive, implies

$$V_\infty > V_{LB1} \qquad\qquad V_{LB1} = \sqrt{\frac{g\cos_M}{\alpha}}, \tag{36}$$

a lower bound on V_∞ that is actually valid for both ascending and non-ascending trajectories.

10. Non-descending trajectories

In non-descending trajectories, all the terms in T_R are non-negative and therefore T_R is always non-negative. The inequalities (29) and (33) or (34) still have to be satisfied. Upon substituting the expression for T_R, from Eq. (31), into (33), the latter inequality can be written in a similar form as (29), namely

$$\frac{\tilde{\lambda}^2}{V_\infty^4} + \frac{(1-s^2)}{R^2} \le F(V_\infty, s) \tag{37}$$

with $F(V_\infty, s) = \dfrac{g^2}{\Gamma V_\infty^2}\dfrac{\left[U(V_\infty) - Ws\right]}{(1-s^2)}$ and $U(V_\infty) = \left\{\dfrac{P_{A\max}(V_\infty)}{V_\infty} - \overline{C}_{D0}V_\infty^2\right\}$,

in which $s = \sin(\theta)$. For jet airplanes, the same inequality holds with $P_{A\max}(V_\infty)/V_\infty$ replaced by $T_{A\max}$. It should be noted that, in both (29) and (37), $\tilde{\lambda}$ and R appear solely as two separate terms on the LHS of the inequality. Clearly if $\tilde{\lambda}$ is increased, 1/R must be decreased and reciprocally; this feature provides some freedom in determining the values of these parameters. The continuability condition requires that (29) and (37) hold with $\tilde{\lambda} = g$, i.e., $\lambda = 0$, at $\theta = \theta_m$ and θ_M. We shall illustrate the analysis procedure by determining a trajectory for a Cessna 182, which starts at the altitude $h_0 = 0$ m, with $\theta_0 = 0$, $\Phi_0 = 0$ and terminates with the ascension angle $\theta_f = \pi/9$.

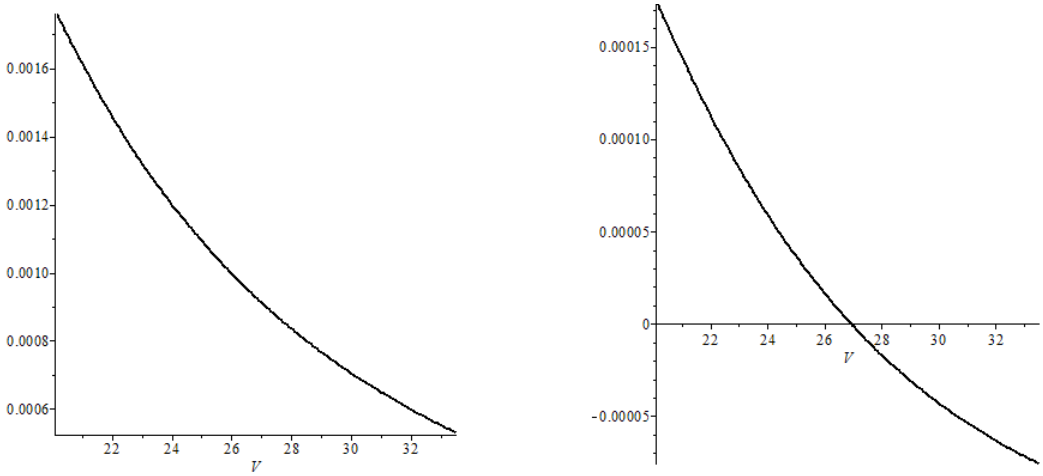

(a) $F(V_\infty, \sin_m) - g^2 V_\infty^{-4}$ (b) $F(V_\infty, \sin_M) - g^2 V_\infty^{-4}$

Fig. 7 Graph of $F(V_\infty, s) - g^2 V_\infty^{-4}$ as a function of V_∞, in (a): when s = $\sin_m$ and in (b) when s = $\sin_M$

10.1 Constraints on V_∞

For the sample trajectory Eq. (36) yields $V_{LB\,1}$ = 20.2 m/s. Since the LHS of (37) is always positive, it is necessary that $U(V_\infty) - Ws > 0 \quad \forall\ s \in [\sin_m, \sin_M]$. This will be the case if and only if it holds with $\sin(\theta)$ is at its maximum value, which is $\sin_M$. Thus, this inequality holds if and only if $U(V_\infty) - W \sin_M > 0$. However, the continuability condition requires even more in that it requires that (37) hold with $\tilde{\lambda}^2 = g^2$, when s = $\sin_m$ and s = $\sin_M$. Thus $F(V_\infty, s)$ must be larger than $\frac{g^2}{V_\infty^4}$ at these values of s. Fig. 7 shows how these quantities vary with V_∞, for the present sample trajectory. It can be determined that their positivity require that $V_\infty \le V_{UB}$, which for the present sample trajectory is 26.9 m/s. The interval of allowed speeds is (V_{LB}, V_{UB}); for our sample trajectory this is (20.3, 26.9) m/s; and therefore, we can select the speed V_∞ = 23 m/s for the trajectory being constructed as example.

10.2 Constraints on $\tilde{\lambda}^2$

(29) and (37) respectively require that

$$\tilde{\lambda}^2 < \tilde{\lambda}^2_{UB1} \qquad \text{with} \quad \tilde{\lambda}^2_{UB1} = V_\infty^4 \gamma^2 (V_\infty, \cos_M). \tag{38}$$

and

$$\tilde{\lambda}^2 < \tilde{\lambda}^2_{UB2} \quad \text{with} \quad \tilde{\lambda}^2_{UB2} = V_\infty^4 F(V_\infty, s_c), \tag{39}$$

in which s_c is the value of s at which F(V_∞, s) is minimum. We note that, if these inequalities hold, it will always be possible to select values of R large enough for (29) and (37) to be satisfied. For the current example $\tilde{\lambda}^2_{UB1}$=162.6 m/s^2. The minimum value of F occurs either at one of the end

points of its s-domain, which are $\sin_m$ and $\sin_M$, or at a critical point, at which its derivative is null. Its derivative is

$$\frac{\partial F(V_\infty, s)}{\partial s} = \frac{g^2}{\Gamma V_\infty^2} \frac{F_1(V_\infty, s)}{(1-s^2)^2} \qquad \text{with} \qquad F_1(V_\infty, s) = \left[-Ws^2 + 2Us - W \right]. \tag{40}$$

The critical points are then the zeros of F_1. As a function of s, F_1 corresponds to a downward concave parabola, with determinant $\Delta_F = 4(U^2\text{-}W^2)$. Its maximum is at s = U/W, which, according to the discussion at the beginning of Section 10.1, is larger than $\sin_M$. Therefore, if $\Delta_F \leq 0$, F_1 is always negative in the interval $\left[\sin_m, \sin_M\right]$, thus F is a monotonically decreasing function of s in this domain, and its minimum value is at $s_c = \sin_M$. If $\Delta_F > 0$, only the smallest root of F_1, s_-, can be in the domain of s; if this is the case, then F is minimum at $s_c = s_-$. The lower bound of $\tilde{\lambda}^2$ is then

$$\tilde{\lambda}_{UB}^2 = Min(\tilde{\lambda}_{UB1}^2, \tilde{\lambda}_{UB2}^2). \tag{41}$$

For the current example $\tilde{\lambda}_{UB2}^2 = 119.7\ \text{m/s}^2$, and this is also the value of $\tilde{\lambda}_{UB}^2$. We then select λ = 0.5 m/s^2 for our example trajectory.

10.3 Constraints on R

Again, (29) and (37) respectively require that

$$R \geq R_{LB1} \qquad \text{with} \qquad \frac{1}{R_{LB1}^2} = \frac{1}{\cos_M^2} \left[\gamma^2(V_\infty, \cos_M) - \frac{\tilde{\lambda}^2}{V_\infty^4} \right], \tag{42}$$

and

$$R \geq R_{LB2} \qquad \text{with} \qquad \frac{1}{R_{LB2}^2} = H(\tilde{\lambda}, V_\infty, s_d), \tag{43}$$

with

$$H(\tilde{\lambda}, V_\infty, s) = \frac{1}{(1-s^2)} \left\{ F(V_\infty, s) - \frac{\tilde{\lambda}^2}{V_\infty^4} \right\} \tag{44}$$

and in which s_d is the value of s at which $H(\tilde{\lambda}, V_\infty, s)$ is minimum. In the present example, R_{LB1} = 70.3 m. The minimum of H is either one of the end points $\sin_m$ and $\sin_M$, or a critical point, at which its derivative with respect to s is null. This derivative is

$$\frac{\partial H(\tilde{\lambda}, V_\infty, s)}{\partial s} = \frac{H_1(\tilde{\lambda}, V_\infty, s)}{V_\infty^2 (1-s^2)^3} \qquad \text{with} \tag{45}$$

$$H_1(\tilde{\lambda}, V_\infty, s) = \left[\frac{2\tilde{\lambda}^2}{V_\infty^2} \right] s^3 - \left[\frac{3g^2 W}{\Gamma} \right] s^2 + \left[-\frac{2\tilde{\lambda}^2}{V_\infty^2} + \frac{4g^2 U}{\Gamma} \right] s - \left[\frac{g^2 W}{\Gamma} \right]. \tag{46}$$

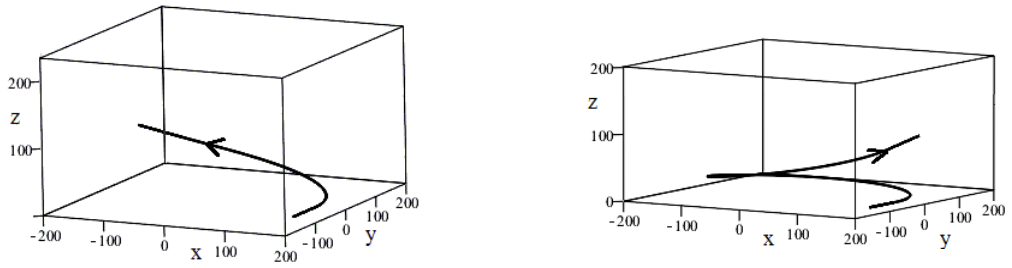

(a) $\lambda = 0.5$ m/s^2 (b) $\lambda = 0.1$ m/s^2

Fig. 8 Two helical trajectory for the Cessna 182, with radius R = 150m, and speed 23 m/s. that starts with $\theta_0 = 0^0$ and terminates with $\theta_f = 20^0$

If $\tilde{\lambda} = 0$, H_1 is a quadratic function of s that corresponds to a concave downward parabola. Its minimum value is therefore either at $s = \sin_m$ or $\sin_M$. If $\tilde{\lambda} \neq 0$, H_1 is a cubic function of s. If it has no real roots in the interval $[\sin_m, \sin_M]$, then the minimum value of $H(\tilde{\lambda}, V_\infty, s)$ is either at $s_d = \sin_m$ or $\sin_M$. If it has real roots in that range, then the minimum of $H(\tilde{\lambda}, V_\infty, s)$ can occur at one of these real roots or at $\sin_m$ or $\sin_M$. In the current example, the only positive real root of H_1 is at s = 14.38, which is not in the interval $[\sin_m, \sin_M]$ and the minimum of H is at $s = \sin_M$, with $R_{LB2} = 134.8$ m. The continuability condition requires that (43) hold with $s = \sin_m$ and $s = \sin_M$, however, this is already guaranteed to be true since H is minimum at $s = s_d$. The lower bound on R is $R_{LB} = \text{Max}\{R_{LB1}, R_{lb2}\}$, so, in the present example, $R_{LB} = 134.8$ m. We select R = 150 m. The resulting trajectory is shown in Fig. 8(a); it last for 16.4 s and, starting at the altitude $h_0 = 0$ m, it terminates at the altitude $h_f = 65.8$ m. Fig. 8(b) shows another trajectory with $\lambda = 0.1$ m/s^2, with the same speed and radius. It lasts for 40.3 s and terminates at $h_f = 81.0$ m.

11. Non-ascending trajectories

Whereas the expression for the thrust required is necessarily non-negative in non-descending trajectories, when the airplane is descending, $\sin(\theta)$ is negative and conditions have to be imposed on the trajectory parameters in order for T_R to remain non-negative. Upon using the expression for T_R given in Eq. (31), the condition $T_R \geq 0$ becomes

$$\frac{\tilde{\lambda}^2}{V_\infty^4} + \frac{(1-s^2)}{R^2} \geq G(V_\infty, s) \qquad \text{with} \qquad G(V_\infty, s) = -\frac{g^2}{\Gamma V_\infty^2} \frac{\left[Ws + \overline{C}_{D0} V_\infty^2\right]}{(1-s^2)}. \tag{47}$$

Obviously, if $\left[Ws + \overline{C}_{D0} V_\infty^2\right] \geq 0$, then (47) is satisfied without any additional requirement on the trajectory parameters. We shall then examine more in details the situation in which this is not the case, and write the two conditions that T_R must satisfy as

$$0 \leq T_R \leq \frac{P_{A\max}(V_\infty)}{V_\infty}. \tag{48}$$

If the airplane were a jet instead of a propeller airplane, the RHS of (48) would be replaced by T_{Amax}. The two (48) can be written in the form

$$G(V_\infty, s) - \frac{(1-s^2)}{R^2} \le \frac{\tilde{\lambda}^2}{V_\infty^4} \le F(V_\infty, s) - \frac{(1-s^2)}{R^2}, \tag{49}$$

The analysis of (49) is made easier by the fact that both of its sides are monotonically decreasing functions of s. Indeed, the derivative of G is

$$\frac{\partial G(V_\infty, s)}{\partial s} = -\frac{g^2}{\Gamma V_\infty^2 (1-s^2)^2}\left[Ws^2 + 2\bar{C}_{D0}V_\infty^2 s + W\right].$$

The term in bracket in the numerator of the RHS is a quadratic polynomial in s; its determinant is $4\left[(\bar{C}_{D0}V_\infty^2)^2 - W^2\right]$, which is always negative because $\left[Ws + \bar{C}_{D0}V_\infty^2\right] < 0$. This polynomial then has no real roots and is always positive; thus, the derivative of G is negative $\forall$ s and G is monotonically decreasing. The derivative of F is given in Eq. (40), and is clearly negative when s $\le$ 0. Similarly, the derivative of $-\frac{(1-s^2)}{R^2}$ is negative for negative values of s. Thus, the two sides of (49) are monotonically decreasing functions of s. This fact implies that the LHS of this inequality holds if and only if it holds at s = $\sin_m$ and its RHS holds if and only if it holds at s = $\sin_M$. The following two inequalities then need to be satisfied

$$G(V_\infty, \sin_m) \le \frac{\tilde{\lambda}^2}{V_\infty^4} + \frac{\cos_M^2}{R^2}. \tag{50}$$

$$\frac{\tilde{\lambda}^2}{V_\infty^4} + \frac{\cos_M^2}{R^2} \le F(V_\infty, \sin_M). \tag{51}$$

We shall illustrate the trajectory construction process with an example trajectory that starts at $\theta_0 = 0^0$ and terminates at $\theta_f = -15^0$.

11.1 Conditions on V∞

Upon comparing (29) and (51), with (50), one can see that it is necessary to have enough space between the RHS of (29) and (51) and the LHS of (50) to insert $\frac{\tilde{\lambda}^2}{V_\infty^4} + \frac{\cos_m^2}{R^2}$ and $\frac{\tilde{\lambda}^2}{V_\infty^4} + \frac{\cos_M^2}{R^2}$ between them. This will always be possible whenever

$$\gamma^2(V_\infty, \cos_M) - G(V_\infty, \sin_m) > 0 \tag{52}$$

and

$$F(V_\infty, \sin_M) - G(V_\infty, \sin_m) > 0, \tag{53}$$

because l and R can always be adjusted appropriately. (52) determines the value of the

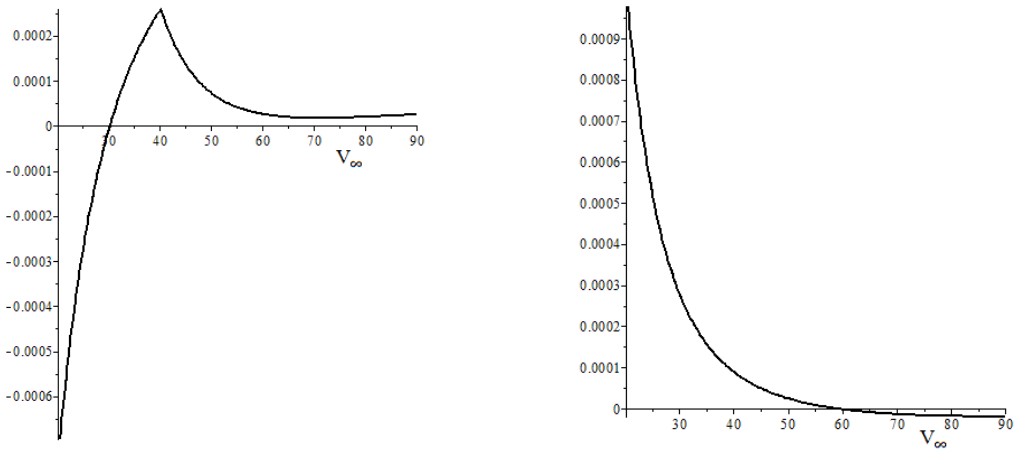

(a) LHS of (52) (b) LHS of (53)

Fig. 9 Determination of the bounds V_{LB2} and V_{UB2} for the Cessna 182 on a trajectory with $\theta_M = 0^0$ and $\theta_m = -15^0$

lower bound V_{LB2}, which for our sample trajectory is 30.3 m/s, and possibly of an upper bound V_{UB1}, which is undefined for the present sample trajectory. Fig. 9(a) shows how the LHS of (52) varies with V_∞. (53) determines the value of the upper bound V_{UB2}, which for our sample trajectory is 58.8 m/s. Fig. 9(b) shows how the LHS of (53) varies with V_∞. The continuability condition is satisfied for (29) whenever $V_\infty \geq V_{LB1}$. It requires that (50) and (51) be satisfied with $\tilde{\lambda}^2$ replaced by g^2. The first inequality will result in a constraint on the value of R and the second in the following inequality

$$0 < \frac{\cos^2_M}{R^2} \leq F(V_\infty, \sin_M) - \frac{g^2}{V_\infty^4}. \tag{54}$$

(54) determines V_{UB3}, which for our sample trajectory is 77.1 m/s. The LHS of (54) behaves very much as shown in Fig. 9(b). The interval of possible speeds is then (V_{LB}, V_{UB}), with V_{LB} = Max(V_{LB1}, V_{LB2}) and V_{UB} = Min((V_{UB1}, $V_{UB2,}$ V_{UB3}). For our sample trajectory this interval is (30.3, 58.8) m/s.

11.2 Conditions on R

The continuability condition applied to (29) and (51) implies that

$$\mathrm{R} \geq \mathrm{R}_{LB1} \text{ with } \quad \frac{1}{R^2_{LB1}} = \frac{\gamma^2(V_\infty, \cos_M) - g^2 V_\infty^{-4}}{\cos^2_M}. \tag{55}$$

and

$$\mathrm{R} \geq \mathrm{R}_{LB2} \text{ with } \quad \frac{1}{R^2_{LB2}} = \frac{F(V_\infty, \sin_M) - g^2 V_\infty^{-4}}{\cos^2_M}. \tag{56}$$

Note that, when $\tilde{\lambda}^2 > g^2$ the bounds on R should be strictly R > R_{LB1} and R > R_{LB2}. Upon comparing (50) and (51), with $\tilde{\lambda}^2$ replaced by g^2, when $\cos_M \neq \cos_m$, there results the inequality

$$R \geq R_{LB3} \qquad \text{with} \qquad \frac{1}{R_{LB3}^2} = \frac{F(V_\infty, \sin_M) - G(V_\infty, \sin_m)}{\cos_M^2 - \cos_m^2}, \tag{57}$$

The continuability condition for (50), yields the following condition on R

$$G(V_\infty, \sin_m) - \frac{g^2}{V_\infty^4} \leq \frac{\cos_m^2}{R^2}. \tag{58}$$

If the LHS of (58) is non-positive, this inequality is satisfied, but if it is positive, it imposes the following constraint on R

$$\mathrm{R} \leq \mathrm{R_{UB}} \quad \text{with} \quad R_{UB}^2 = \frac{\cos_m^2}{G(V_\infty, \sin_m) - g^2 V_\infty^{-4}}. \tag{59}$$

The bounds on R are then R_{LB} = Max(R_{LB1}, R_{LB2}, R_{LB3}) and R_{UB}. For the Cessna 182, with the speed V_∞ = 45 m/s, R_{LB} = 66.5 m and R_{UB} = 72.6 m. We shall select R = 70 m/s for our sample trajectory.

11.3 Conditions on λ

We shall treat separately the two cases in which $\tilde{\lambda}^2 \leq g^2$ and $\tilde{\lambda}^2 > g^2$.

Case $\tilde{\lambda}^2 \leq g^2$

In this case, (35) implies that (29) is satisfied and (51), with g^2 instead of $\tilde{\lambda}^2$, implies that (51) is satisfied. There then remains only to ensure that (50) holds, that is

$$\left[G(V_\infty, \sin_m) - \frac{\cos_m^2}{R^2} \right] V_\infty^4 \leq \tilde{\lambda}^2 \leq g^2. \tag{60}$$

If the LHS of (60) is non-positive, then this inequality holds for all values of λ such that $\tilde{\lambda}^2 \leq g^2$. If it is positive, then the LHS of (60) is a lower bound $\tilde{\lambda}_{LB}^2$ on $\tilde{\lambda}^2$, and (60) becomes $\tilde{\lambda}_{LB}^2 \leq \tilde{\lambda}^2 \leq g^2$. For the sample trajectory considered, the LHS of (60) is positive, and $\tilde{\lambda}_{LB}^2 = 40.55\ \mathrm{m^2/s^4}$. We can then select λ = -0.5 m/s^2. Fig. 10(a) shows the trajectory that corresponds to the selected values of the parameters. This trajectory starts at the altitude h_0 = 500 m, finishes at h_f = 359.6 m, and lasts 23.8 s. When λ = -1.5 m/s^2 is selected, the trajectory ends at h_f = 453.2 m and lasts 7.9 s. Fig. 10(b) shows this trajectory.

Case $\tilde{\lambda}^2 > g^2$

(29) and (51) can be written as

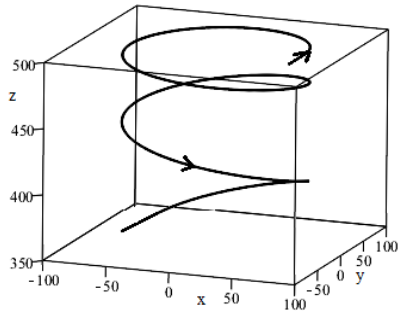

(a) With λ = -0.5 m/s^2

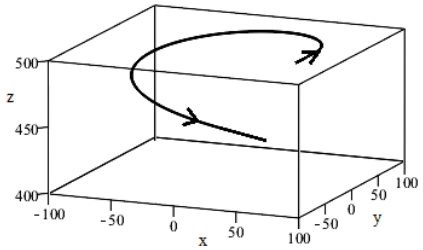

(b) With λ = -1.5 m/s^2

Fig. 10 Two descending trajectories for the Cessna 182, which start at q_0 = and end at $q_f = -15^0$, with V_∞ = 45 m/s, R= 70 m, and two different rates of inclination change

$$\frac{\tilde{\lambda}^2 - g^2}{V_\infty^4} + \frac{\cos_M^2}{R^2} \le \gamma^2(V_\infty, \cos_M) - \frac{g^2}{V_\infty^4}. \tag{61}$$

$$\frac{\tilde{\lambda}^2 - g^2}{V_\infty^4} + \frac{\cos_M^2}{R^2} \le F(V_\infty, \sin_M) - \frac{g^2}{V_\infty^4}. \tag{62}$$

Since the LHS of (61) and (62) are larger than those of (35) and (54), it is necessary to require that R be strictly larger than the two bounds R_{LB1} and R_{LB2}. This requirement ensures that there will be a gap between $\frac{\cos_M^2}{R^2}$ and the RHS of (61) and (62). It will then always be possible to select $(\tilde{\lambda}^2 - g^2)$ small enough that adding the term $\frac{\tilde{\lambda}^2 - g^2}{V_\infty^4}$ to $\frac{\cos_M^2}{R^2}$ will yield a value smaller than the RHS of (61) and (62). We note that, since in the present case, $\tilde{\lambda}^2 > g^2$, 50) will always be satisfied if it is satisfied with $\tilde{\lambda}^2$ replaced by g^2, i.e., when in Eq. (58) is satisfied. (61) and (62) can be written as

$$\tilde{\lambda}^2 \le \tilde{\lambda}_{UB1}^2 \quad \text{with} \quad \tilde{\lambda}_{UB1}^2 = V_\infty^4 \left[\gamma^2(V_\infty, \cos_M) - \frac{\cos_M^2}{R^2} \right] \tag{63}$$

and

$$\tilde{\lambda}^2 \le \tilde{\lambda}_{UB2}^2 \quad \text{with} \quad \tilde{\lambda}_{UB2}^2 = V_\infty^4 \left[F(V_\infty, \sin_M) - \frac{\cos_M^2}{R^2} \right]. \tag{64}$$

Thus, λ must be selected such that

$$g^2 \le \tilde{\lambda}^2 \le \tilde{\lambda}_{UB}^2 \quad \text{with} \quad \tilde{\lambda}_{UB}^2 = Min(\tilde{\lambda}_{UB1}^2, \tilde{\lambda}_{UB2}^2). \tag{65}$$

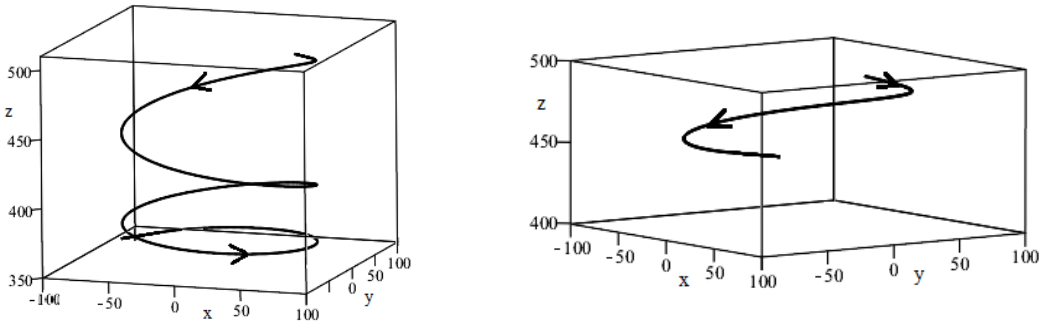

(a) With $\lambda = 0.5$ m/s^2 (b) With $\lambda = 1.5$ m/s^2

Fig. 11 Two descending trajectories for the Cessna 182, which start at $q_0 = -15^0$ and terminate at $q_f=0$, with $V_\infty = 45$ m/s, R= 70, and two different inclination change rates

For the sample trajectory with $q_0 = -15^0$, $q_f = 0^0$, R = 70 m, and $V_\infty = 45$ m/s, $\tilde{\lambda}^2_{UB}$=40.55 m^2/s^4. Thus, a possibility would be $\lambda = 0.5$ m/s^2, which yields the trajectory shown in Fig. 11(a). It starts at an altitude of 500 m, lasts 23.8 s and ends at the altitude of 359.6 m. Another possibility would be $\lambda = 1.5$ m/s^2, which yield the trajectory shown in Fig. 11(b). It lasts 7.9 s and terminates at the altitude of 453.2 m.

12. Speed interval tables for non-descending trajectories

In trajectory planning, the problem is most often posed as that of constructing flyable trajectories with given initial and a final angles of inclination for the helix. In non-descending trajectories, both of these angles are non-negative and in non-ascending trajectories, both are non-positive. We note that, for airplanes with propellers, the flyability analysis requires a representation of the function P_{Amax} in terms of V_∞, possibly as splines or as a table of values. All the calculations are performed with algebraic formulas, except for the determination of the range of allowed speeds, which requires a numerical solution with P_{Amax}. Consequently, disposing of tables of allowed speed values, would appreciably accelerate the calculations. Such tables are easily constructed, as we will show below, for our selected sample planes, which are the Cessna 182, the Silver Fox like unmanned UAV and the F-16 Fighting Falcon. The characteristics that we use for these three airplanes are given in Appendix A.

These tables provide the intervals of speeds for which helical trajectories, of the type discussed in this report, are flyable. The first two lines of the table give the value of the lower bound on the speed: V_{LB}, for various smallest angles θ_m. The last two lines of the table give the value of the upper bound on the speed: V_{UB}, for various largest angles θ_M. Thus, for example, if a trajectory should have inclination that vary between $\theta_m = 0^0$, and $\theta_M = 20^0$, the interval of allowed speeds would be (20.2, 26.9) m/s. It is remarkable that V_{LB} does not vary much as θ_m varies from 0 to 20 degrees; this is due to the fact that V_{LB} depends on $\cos(\theta)$ which is close to 1 for all these angles. We note that if a trajectory is flyable with starting inclination of θ_m and final inclination of θ_M, the trajectory that starts with the inclination θ_M and terminates with inclination θ_m is also flyable. We note that a simple linear extrapolation between the values given in the table would give excellent results. Flyable trajectories exist for all the speeds in the intervals shown in the tables.

Table 1 Speed intervals of flyable trajectories for the Cessna 182; θ_m is the smallest angle and V_{LB} the lower bound on the speed for this angle, θ_M is the largest angle and V_{UB} is the upper bound of the speed for that angle

θ_m (deg)	0	5	10	15	20
V_{LB} (m/s)	20.2	20.2	20.1	19.9	19.6

θ_M (deg)	0	5	10	15	20
V_{UB} (m/s)	77.1	65.8	53.6	40.7	26.9

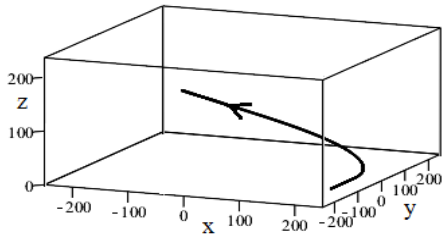

(a) Cessna 182 trajectory, from 0^0 to 20^0

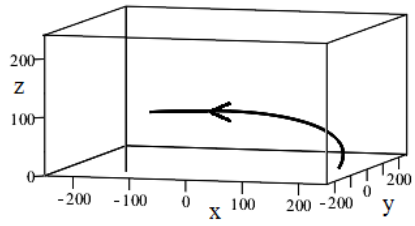

(b) Cessna 182 trajectory, from 20^0 to 0^0

Fig. 12 Trajectories of the Cessna 182 that correspond to the examples in the text

12.1 Speed interval table for the Cessna 182

For example, according to this table, a trajectory can be constructed with $\theta_0 = 0^0$ and $\theta_f = 20^0$, with speed $V_\infty = 24$ m/s. Eq. (38) yields $\tilde{\lambda}^2_{UB1} = 192.8$ m^2/s^4. The determinant Δ_F, defined after Eq. (40) is negative, and thus, F is minimum at s = $\sin_M$. (39) then yields $\tilde{\lambda}^2_{UB2} = 115.6$ m^2/s^4. Therefore, $\tilde{\lambda}^2 < 192.8$ m^2/s^4, and we can take $\lambda = 0.5$ m/s^2. Eq. (42) yields $R_{LB1} = 58.2$ m. The real root of H_1 is 5.8, which is not in the interval $[\sin_m, \sin_M]$; a verification shows that H is minimum at s = $\sin_M$, yielding $R_{LB2} = 174.9$ m. Thus $R \leq 174.9$ m and a possible choice is R = 200 m. The resulting trajectory lasts 17.1 s; it starts at $h_0 = 0$ m and terminates at $h_f = 71.7$ m. It is shown in Fig. 12(a). The reciprocal trajectory in which the initial angle of inclination is 20^0, and the final angle is 0^0, with $l = -0.5$ m/s^2, and the same speed and radius, lasts the same amount of time and has the same length. It is shown in Fig. 12(b).

12.2 Speed interval table for the silver fox like UAV

Table 2 Speed intervals of flyable trajectories for the Silver Fox-like UAV; q_m is the smallest angle and V_{LB} the lower bound on the speed for this angle, q_M is the largest angle and V_{UB} is the upper bound of the speed for that angle

θ_M (deg)	0	10	20	30	40	50
V_{UB} (m/s)	13.8	13.7	13.4	12.8	12.1	11.1

θ_M (deg)	0	10	20	30	40	50
V_{UB} (m/s)	56.3	50.9	42.5	33.5	24.2	14.4

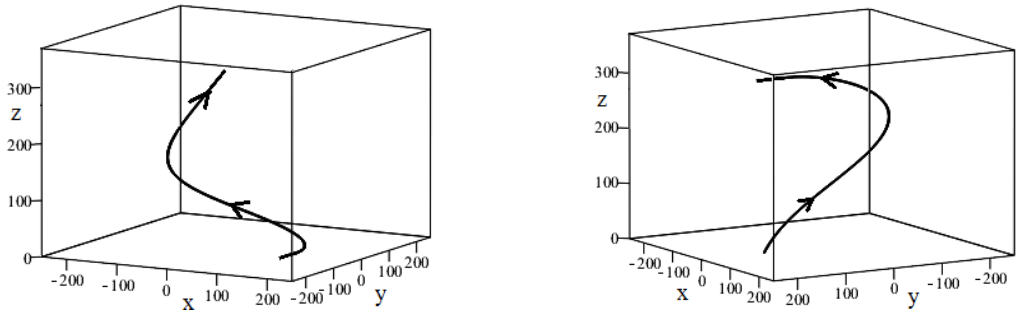

(a) Silver Fox-like trajectory, from 0^0 to 50^0 (b) Silver Fox-like trajectory, from 50^0 to 0^0

Fig. 13 Trajectories of the Silver Fox-like UAV that correspond to the examples in the text

Table 3 Speed intervals of flyable trajectories for the F-16 Fighting Falcon; θ_m is the smallest angle and V_{LB} the lower bound on the speed for this angle, θ_M is the largest angle and V_{UB} is the upper bound of the speed for that angle

θ_m (deg)	0	20	40	60	80
V_{LB} (m/s)	62.8	60.9	55.0	44.4	26.2

θ_M (deg)	0	20	40	60	80
V_{UB} (m/s)	543.0	448.8	345.4	242.0	163.9

For example, according to this table, a trajectory can be constructed with $\theta_0 = 0^0$ and $\theta_f = 50^0$ and $V_\infty = 14$ m/s. Eq. (38) then yields $\tilde{\lambda}^2_{UB1} = 103.3 \text{ m}^2/\text{s}^4$. The determinant Δ_F, is negative, and thus, F is minimum at $s = \sin_M$. (39) then yields $\tilde{\lambda}^2_{UB2} = 110.3 \text{ m}^2/\text{s}^4$, so that $\tilde{\lambda}^2 < 103.3$ m^2/s^4 and a possible choice is $\lambda = 0.3$ m/s^2. Eq. (42) yields $R_{LB1} = 109.9$ m. The real root of H_1 is 6.8, which is not in the interval $[\sin_m, \sin_M]$; a verification shows that H is minimum at $s = \sin_M$, yielding $R_{LB2} = 43.6$ m. Thus $R_{LB} = 109.9$ m and a possible choice is R = 120 m. The resulting trajectory lasts 47.2 s, it starts at $h_0 = 0$ m and terminates at $h_f = 288.7$ m. It is shown in Fig. 13(a). The reciprocal trajectory in which the angle of inclination varies from 50^0 to 0^0, with $\lambda = -0.3$ m/s^2, and the same speed and radius, lasts the same amount of time and has the same length. It is shown in Fig. 13(b).

12.3 Speed interval table for the Lockeed-Martin F-16

For example, according to this table, a trajectory can be constructed with $\theta_0 = 0^0$ and $\theta_f = 80^0$ and $V_\infty = 100$ m/s. Eq. (38) then yields $\tilde{\lambda}^2_{UB1} = 619.1 \text{ m}^2/\text{s}^4$. The determinant Δ_F, defined after Eq. (40) is positive and F has its minimum at its smallest root $s_- = 0.735$. (39) then yields $\tilde{\lambda}^2_{UB2} = 830.6$ m^2/s^4 and therefore, $\tilde{\lambda}^2 < 619.1$ m^2/s^4, and we can then take $\lambda = 5$ m/s^2. Eq. (42) yields $R_{LB1} = 86.9$ m. H_1 has three real roots; only one of them is in the interval $[\sin_m, \sin_M]$; it is at $s_d = 0.356$, and H is minimum at this point. Eq. (43) then yields $R_{LB2} = 342.6$ m. Thus $R \geq 341.6$ m and a possible choice is R = 350 m. The resulting trajectory lasts 48.7 s, it starts at $h_0 = 0$ m and terminates at $h_f = 3501.4$ m. It is shown in Fig. 14(a). The reciprocal trajectory in which the angle

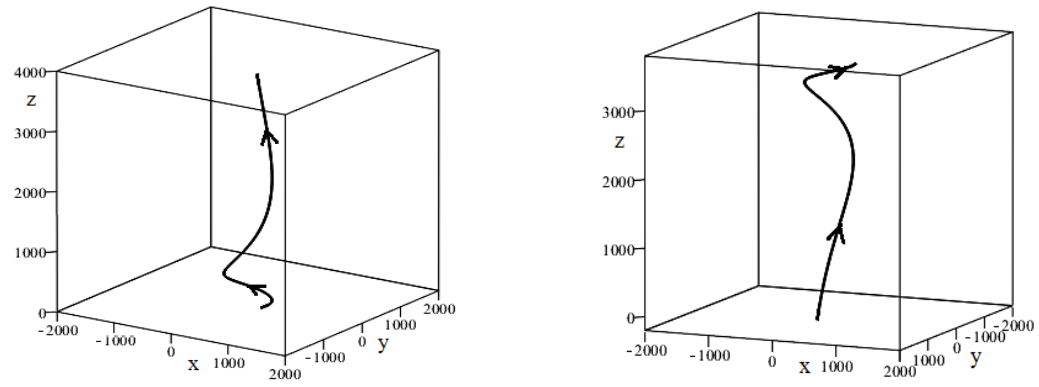

(a) F-16 trajectory with $\theta_0 = 0^0$, $\theta_f = 80^0$ (b) F-16 trajectory with $\theta_0 = 80^0$, $\theta_f = 0^0$

Fig. 14 Trajectories of the F-16 that correspond to the examples in the text

Table 4 Speed intervals of flyable trajectories for the Cessna 182; initial angles are in the columns and final angles in the rows

θ_f \ θ_0	0	-5	-10	-15	-20
0	20.7, 77.1				
-5	20.7, 77.1	20.6, 82.3			
-10	24.5, 77.1	24.3, 82.3	24.1, 99.0		
-15	30.3, 58.8	30.2, 82.3	30.0, 99.0	29.5, 109.0	
-20	X	35.6, 48.6	35.3, 49.5 87.3, 94.2	34.7, 50.9 86.5, 109.0	33.8, 53.2 85.0, 118.3

of inclination varies from 80^0 to 0^0, with λ = -5 m/s^2, and the same speed and radius, lasts the same amount of time and terminates at the same altitude h_f. It is shown in Fig. 14(b). It should however be mentioned that with such a difference in altitude, the variation of the air density should be taken into account in the calculations. This was not done here, and therefore, the above results should be considered as an approximation of the real situation.

13. Speed interval tables for non-ascending trajectories

We now give examples of speed interval tables for non-ascending trajectories. They are in a different format than those of Section 12, because, for these trajectories, the lower bound and upper bound on speed do not depend only on θ_m and θ_M. Columns and rows correspond respectively to initial and final angles of inclination. The table is symmetric about the diagonal, and thus, we did not repeat the entries in the cells where they could be obtained by symmetry.

13.1 Speed interval table for the Cessna 182

It is worth remarking that for certain combination of angles, there are two disjoint speed intervals. This phenomenon was already mentioned in Section 8.1 of Labonté (2017). It was explained that at lower speeds, it is the lift induced drag that dominates and cancels gravity so that

Table 5 Speed intervals of flyable trajectories for the Silver Fox-like UAV; initial angles are in the columns and final angles in the rows

θ_f \ θ_0	0	-5	-10	-15	-20	-25
0	14.1, 56.3					
-5	14.4, 56.3	14.2, 58.4				
-10	20.5, 56.3	20.4, 58.4	20.2, 60.4			
-15	25.3, 56.3	25.2, 58.4	25.0, 60.4	24.7, 62.2		
-20	29.7, 56.1	29.6, 58.4	29.4, 60.4	28.9, 62.2	28.4, 63.8	
-25	X	X	56.8, 59.0	56.4, 61.8	55.8, 63.8	63.8, 65.3

Table 6 Speed intervals of flyable trajectories for the F-16 Fighting Falcon; initial angles are in the columns and final angles in the rows. Colored cells contain speeds larger than that of sound

θ_f \ θ_0	0	-20	-40	-60	-80
0	64.3, 543.0				
-20	87.9, 543.0	83.0, 623.2			
-40	144.8, 543.0	137.0, 623.2	113.8, 686.0		
-60	465.2, 543.0	461.6, 623.2	446.1, 686.0	132.1, 729.1	
-80	517.4, 543.0	516.1, 623.2	515.0, 686.0	510.4, 729.1	140.7, 329.4 400.0, 751.1

the airplane can keep descending at constant speed. Then, at higher speeds, it is the parasite drag that dominates and cancels gravity so that the airplane can descend at constant speed.

It might be found intriguing that, according to this table, the airplane can fly on a helical trajectory with an inclination that goes from 0^0 to -5^0 and on one that goes from -5^0 to -20^0, but cannot fly on one that varies from 0^0 to -20^0. The explanation of this apparent paradox is simply that the two first trajectories are possible separately, but they would not have the same radius nor the same speed, as can be seen in the table.

13.2 Speed interval table for the silver fox-like UAV

According to this table, an example of flyable trajectory would be one in which the inclination angle varies from -15^0 to 0^0. According to Table 5, a possible speed would be $V_\infty = 30$ m/s. (55)-(59) yield $R_{LB} = 20.8$ m and $R_{UB} = 26.1$ m; the interval of possible values for R is thus small, nevertheless a possible radius would be R = 24.0 m. (65) yields $\lambda_{UB} = 23.9$ m/s^2 so that a possible choice is $\lambda = 0.5$ m/s^2. The resulting trajectory takes 15.9 s, starts at 100 m and terminates at 37.6 m. It is shown in Fig. 15(a).

13.3 Speed interval table for the F-16 fighting falcon

We note that many of the speeds intervals in this table contain speeds larger than the speed of sound (340.3 m/s). Thus, the formulas we have derived not very accurate at these speeds, because the dynamics of airplanes at supersonic speeds is quite different than those at subsonic speeds (Stengel 2016). Cells of the table containing only speeds larger than that of sound are colored in grey.

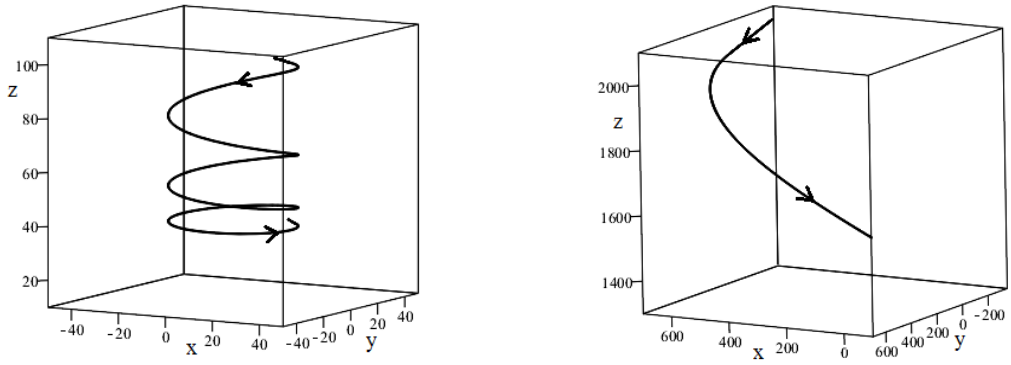

(a) Silver Fox-like UAV trajectory (b) F-16 trajectory

Fig. 15 Trajectories of the Silver Fox like UAV and the F-16 given as examples in the text

When flying on steep trajectories, the F-16 would travel long vertical distances during which the air density and temperature would vary considerably. In the present study, we did not take into account these changes. The values in the table therefore only give some indication of what can be expected to be possible, when all the relevant factors are taken into account.

According to the table, an example of trajectory would have an angle of inclination varying from -10^0 to -30^0. A possible speed would then be V_∞ = 200 m/s. (55)-(59) then yield R_{LB} = 656.3 m and R_{UB} = 737.5 m, and a possible radius would be R = 700 m. (60) then imposes no constraint on l since its LHS is negative; a possible choice is λ = -9.6 m/s^2. The resulting trajectory starts at h_0 = 2000 m and terminates at h_f = 1464 m; it lasts 7.8 s. It is shown in Fig. 15(b).

14. Conclusions

There are three important results presented in this article.

• The first one is the description of a new type of constant speed helical trajectory with varying ascension rate, for which the airplane equations of motion are exactly solvable. The altitude varies almost linearly on this trajectory. Such trajectories can be used very advantageously in trajectory planning, for connecting rectilinear, circular or helical segments; since it requires much less calculations than other smoothing connections. They are also valuable by themselves in situations in which an airplane has to land or take off in a limited space.

• The second one is the derivation of the constraints on the geometrical parameters of the trajectory that result from the bounds on the dynamical abilities of the airplane. It takes into account its load factor, its lift coefficient, its thrust and power. Formulas are given for determining the possible angles of inclination of the trajectory, its minimum radius, the minimum and maximum speeds, the flight time required, and the altitude difference between the final and initial ascension angles.

• The third one is the explanation of a method for constructing tables that list the intervals of speeds, for which helical trajectories with given initial and final angles of ascension are flyable. Such talbes, together with the formulas derived, will be very useful for on-board trajectory planning, even when small microcontrollers are used. They can be calculated beforehand, and stored in the memory of the processor, where they would not require much space. Examples of

such tables are given for three very different airplanes, namely the Cessna 182 Skylane, the Silver Fox UAV and the F-16 Fighting Falcon.

We believe that the type of variable ascension angle helical trajectory, as well as the formulas related to it, are original in that they have never been published before. They will find a definite usefulness in airplane trajectory planning. They also constitute, in themselves, an important tool for the analysis of airplane performances.

References

Aeronautics Learning Labratory for Science Technology and Research (ALLSTAR) of the Florida International University (2011), *Propeller Aircraft Performance and The Bootstrap Approach*.

Airliners.net (2015), Santa Monica, California, U.S.A.
<http://www.airliners.net/aircraft-data/stats.main?id=145>.

Ambrosino, G., Ariola, M., Ciniglio, U., Corraro, F., De Lellis, E. and Pironti, A. (2009), "Path generation and tracking in 3-D for UAVs", *IEEE Trans. Contr. Syst. Technol.*, **17**(4), 980-988.

Anderson, J.D. Jr (2000), *Introduction to Flight*, 4th Edition, McGraw-Hill Series in Aeronautical and Aerospace Engineering, Toronto, Ontario, Canada.

Babaei, A.R. and Mortazavi, M. (2010), "Three-dimensional curvature-constrained trajectory planning based on in-flight waypoints", *J. Aircraft*, **47**(4), 1391-1398.

Beard, R.W. and McLain, T.W. (2015), "Implementing dubins airplane paths on fixed-wing UAVs", Handbook for Unmanned Aerial Vehicles, Section XII, 1677-1701, Springer, the Netherlands.

Boukraa, D., Bestaoui, Y. and Azouz, N. (2006), "A new approach to trajectories planner design for a subsonic autonomous aerial fixed wing vehicle", *Proceedings of the 2006 American Control Conference*, Minneapolis, Minnesota, U.S.A., June.

Cavcar, M. (2004), *Propeller*, http://home.anadolu.edu.tr/~mcavcar/common/Propeller.pdf.
Anadolu University, School of Civil Aviation, Eskisehir, Turkey.

Chandler, P., Rasmussen, S. and Pachter, M. (2000), "UAV cooperative path planning", *Proceedings of the AIAA Guidance, Navigation, and Control Conference*, Denver, Colorado, U.S.A., August.

Chitsaz, H. and LaValle, S.M. (2007), "Time-optimal paths for a dubins airplane", *Proceedings of the 46th IEEE Conference on Decision and Control*, New Orleans, Luisiana, U.S.A., December.

Commercial Aviation Safety Team (CAST), (2011), *Propeller Operation and Malfunctions Basic Familiarization for Flight Crews*, http://www.cast-safety.org/pdf/4_propeller_fundamentals.pdf.

Cowley, W.L. and Levy, H. (1920), *Aeronautics Theory and Experiment*, 2nd Edition, Edward Arnold, London, U.K.

Crawford, D.J. and Bowles, R.L. (1975), *Automatic Guidance and Control of a Transport Aircraft During a Helical Landing Approach*, NASA technical note D-7980, NASA Langley Research Center, Hampton, Va., September.

Dai, R. and Cochran, J.E. (2009), "Three-dimensional trajectory optimization in constrained airspace", *J. Aircr.*, **46**(2), 627-634.

Dubins, L.E. (1957), "On curves of minimal length with a constraint on average curvature and with prescribed initial and terminal positions and tangents", *Am. J. Math.*, **79**, 497-516.

Etkin, B. (1992), *Dynamics of Atmospheric Flight*, John Wiley and Sons, Inc., New York, U.S.A.

Filippone, A. (2000), "Data and performances of selected aircraft and rotorcraft", *Prog. Aerosp. Sci.*, **36**, 629-654.

Frazzoli, M.A., Dahleh, and Feron, E. (2005), "Maneuver-based motion planning for nonlinear systems with symmetries", *IEEE Trans. Robot.*, **21**(6), 1077-1091.

Goman, M.G., Khramtsovsky, A.V. and Kolesnikov, E.N. (2008), "Evaluation of aircraft performance and maneuverability by computation of attainable equilibrium sets", *J. Guid. Contr. Dyn.*, **31**(2), 329-339.

Granelli, F. (2007), *Carl Goldberg Falcon 56*, The Academy of Model Aeronautics' Sport Aviator, The E-

Zine for the Newer RC Pilot, December, http://masportaviator.com/2007/12/01/carl-goldberg-falcon-56/.
Horizon Hobby (2017), https://www.horizonhobby.com/product/airplanes/airplane-accessories/airplane-engines-15042--1/gt80-twin-cylinder-(488-cu-in)-zene80t.
Hota, S and Ghose, D. (2010), "Optimal geometrical path in 3D with curvature constraint", *Proceedings of the IEEE/RSJ International Conference on Intelligent Robots and Systems (IROS)*, Taipei, Taiwan, October.
Hwangbo, M., Kuffner, J. and Kanade, T. (2007), "Efficient two-phase 3D motion planning for small fixed-wing UAVs", *Proceedings of the IEEE International Conference on Robotics and Automation*, Rome, Italy, April.
Jia, D. and Vagners, J. (2004), "Parallel evolutionary algorithms for UAV path planning", *Proceedings of the AIAA 1st Intelligent Systems Technical Conference*, Chicago, Illinois, September.
Judd, K.B. (2001), "Trajectory planning strategies for unmanned air vehicles", M.Sc. Dissertation, Brigham Young University, Provo, U.S.A.
Labonté, G. (2012), "Formulas for the fuel of climbing propeller driven planes", *Aircr. Eng. Aerosp. Technol.*, **84**(1), 23-36.
Labonté, G. (2015), "Simple formulas for the fuel of climbing propeller driven airplanes", *Adv. Aircr. Spacecr. Sci.*, **2**(4), 367-389.
Labonté, G. (2016), "Airplanes at constant speeds on inclined circular trajectories", *Adv. Aircr. Spacecr. Sci.*, **3**(4), 399-425.
Labonté, G. (2017), "The feasible constant speed helical trajectories for propeller driven airplanes", *Adv. Aircr. Spacecr. Sci.*, **4**(4), 371-399.
Li, X., Xie, J., Cai, M., Xie, M. Wang, Z. (2009), "Path planning for UAV based on improved A* algorithm", *Proceedings of the 9th International Conference on Electronic Measurement & Instruments*, Beijing, China, August.
Lockheed-Martin (2015), *F-16 Specifications*
<http://lockheedmartin.com/us/products/f16/F-16Specifications.html>.
Mair, W.A. and Birdsall, D.L. (1992), *Aircraft Performance*, Cambridge Aerospace Series 5, Cambridge University Press, Cambridge, G.B.
McIver, J. (2003), *Cessna Skyhawk II /100, Performance Assessment*, Temporal Images, Melbourne, Australia, http://www.temporal.com.au/c172.pdf.
Narayan, P.P., Wu, P.P. and Campbell, D.A. (2008), "Unmanning UAVs-addressing challenges in on-board planning and decision making", *Proceedings of the 1st International Conference on Humans Operating Unmanned Systems*, Telecom Bretagne, Brest, France, September.
Nikolos, I.K., Tsourveloudis, N.C. and Valavanis, K.P. (2003), "Evolutionary algorithm based 3-D path planner for UAV navigation", *IEEE Trans. Syst. Man. Cybernet. Part B: Cybernet.*, **33**(6), 898-912.
Phillips, W.F. (2004), *Mechanics of Flight*, John Wiley & Sons, Inc., Hoboken, New Jersey, U.S.A.
Roberge, V., Tarbouchi, M. and Labonté, G (2012), "Comparison of parallel genetic algorithm and particle swarm optimization for real-time UAV path planning", *IEEE Trans. Industr. Informat.*, **9**(1), 132-141.
Roud, O. and Bruckert D. (2006), *Cessna 182 Training Manual*, Red Sky Ventures and Memel CATS, Second Edition 2011, Windhoek, Namibia.
Sadraey, M.H. (2013), *Aircraft Design: A Systems Engineering Approach*, Aerospace Series, John Wiley & Sons Ltd, Toronto, Ontario, Canada.
Stengel, R. (2016), *Problems of High Speed and Altitude*.
<https://www.princeton.edu/~stengel/MAE331Lecture22.pdf>.
Tsiotras, P. Bakolas, E. and Zhao, Y. (2011), "Initial guess generation for aircraft landing trajectory optimization", *Proceedings of the AIAA Guidance, Navigation, and Control Conference,* Portland Oregon, August.
UAVGLOBAL Unmanned Systems and Manufacturers (2016), *BAE Systems Silver Fox*.
<http://www.uavglobal.com/bae-systems-silver-fox/>.
Von Mises, R. (1945), *Theory of Flight*, Dover Publications Inc., New York, U.S.A.
Yang, K. and Sukkarieh, S. (2010), "An analytical continuous-curvature path-smoothing algorithm", *IEEE*

Trans. *Robot*., **26**, 561-568.
Zheng, C., Ding, M. and Zhou, C. (2003), "Real-time route planning for unmanned air vehicle with an evolutionary algorithm", *J. Patt*. *Recog*. *Artif*. *Intellig*., **17**(1), 63-81.

EC

Nomenclature

a speed of sound in air. At altitude h, a(h) = $\sqrt{\gamma RT(h)}$. At sea level, a(0) = 340.3029 m/s

a_1 absolute value of the slope of the temperature as a function of altitude, below 11 km, $a_1 = 6.5\times 10^{-3}$ K/m

AFR air fuel ratio (about 14.7)

AR aspect ratio $=b^2/S$

b wingspan

c specific fuel consumption in Newton per Watt-second, that is in m^{-1}

C_D global drag coefficient for the aircraft = $C_{D0} + \frac{C_L^2}{\pi e AR}$ (Drag polar)

C_{D0} global drag coefficient at zero lift

C_L global lift coefficient for the aircraft

D drag = $\frac{1}{2}\rho_\infty S C_D V_\infty^2$

e Oswald's efficiency factor

g gravitational constant = 9.8 m/s^2

h altitude of airplane

h_c service ceiling

L lift = $\frac{1}{2}\rho_\infty S C_L V_\infty^2$

P power of the engine in Watt

R specific gas constant for air = 287.058 J/(kg K)

S wing area

t time variable

T_s temperature at sea level = 288.16 K

T(h) temperature at altitude h

v3 vertical component of airplane velocity

V_∞ airplane speed with respect to the undisturbed air in front of it

V_{NE} speed never to be exceeded

W weight of the airplane

W_1 weight of the empty airplane

W_f maximum weight of fuel

W_0 maximum take-off weight (MTOW)

g ratio of the constant pressure specific heat to the constant volume specific heat $=c_P/c_V$ = 1.4 for air

h propeller efficiency

r_s air density at sea level = 1.225 kg/m^3

$r_\infty(h)$ density of undisturbed air in front of airplane, at altitude h, $\rho_s\left[\frac{T(h)}{T_s}\right]^{4,2433}$

Appendix A: Reference airplanes

We note that there could be small differences between the values we list here and the actual values for a particular model of these airplanes. We used values that were available on the internet or were estimated from the values for similar airplanes. These data are quite adequate for our purpose that is to illustrate the calculations involved in the formulas we have derived.

The thrust of the Cessna 182 and that of the C-130 Hercules is provided by a reciprocating engine with constant speed propeller; that of the Silver Fox by a reciprocating engine with a fixed pitch propeller. We recall that the efficiency of the propeller is a function of the advance ratio J, defined as

$$J = \frac{V_\infty}{N\,D}$$

in which N is its number of revolution per second and D is its diameter. Thus, the maximum power available P_{Amax} will depend on the speed, according to the equation

$$P_{A\max} = \eta(J) P_{\max}$$

The dependence of h on J for a constant speed propeller has the general features shown in Fig. 12(a). This curve approximates that given in Cavcar (2004) by the following quadratic expressions

$$\eta(J) = \left[\frac{0.663}{0.640}\right]\left[J - 0.8\right]^2 + 0.8 \quad \forall\ \mathrm{J} \le 0.8.$$

$$\eta(J) = 0.8 \quad \forall\ \mathrm{J} > 0.8.$$

The dependence of h on J for a fixed pitch propeller has the general features shown in Fig. 12(b). This curve approximates that given in the Aeronautics Learning Laboratory for Science Technology and Research (ALLSTAR) of the Florida International University (2011) by the following quadratic expressions

$$\eta(J) = -\left[\frac{0.83}{0.49}\right]\left[J - 0.70\right]^2 + 0.83 \ \forall\ \mathrm{J} \le 0.7.$$

$$\eta(J) = -\left[\frac{0.83}{0.06}\right]\left[J - 0.70\right]^2 + 0.83 \ \forall\ \mathrm{J} > 0.7.$$

Note that the propeller efficiency of this fixed pitch propellers goes to 0 at V_∞ = 66.1 m/s and becomes negative after that. Although a negative propeller efficiency might be desirable to slow down the airplane when it descends, it is not recommended to let this happens. When this happens, the propeller drives the engine and damage to the engine may result [see for example the Commercial Aviation Safety Team document (2011). We shall therefore not allow speeds larger than that value.

A.1 Cessna 182 skylane

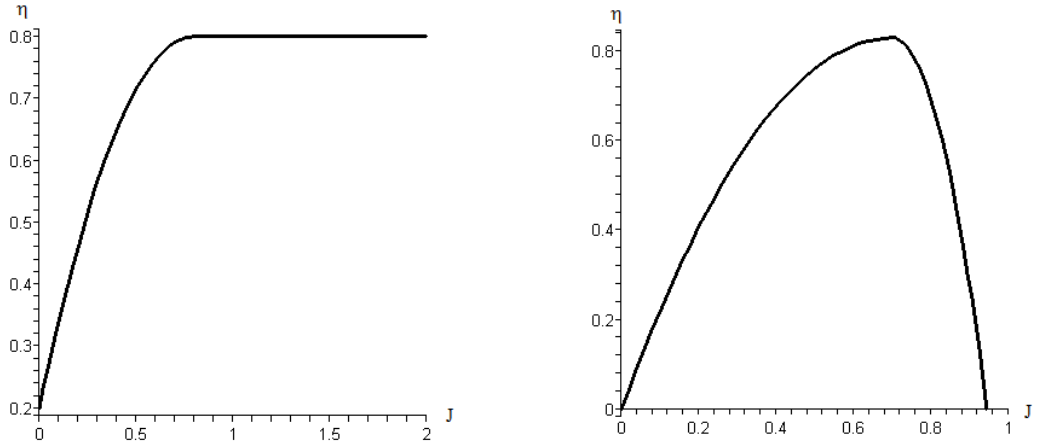

(a) Constant speed propeller (b) Constant pitch propeller

Fig. 16 Typical efficiency factor h as a function of the advance ratio J

The parameters listed are W_1 = the weight of the empty airplane, W_0 = the maximum take-off weight, W_F = the maximum weight of fuel, b = the wingspan, S = the wing area, e = Oswald's efficiency factor, C_{Lmax} = the maximum global lift coefficient, C_{D0} = the global drag coefficient at zero lift, n_{max} and n_{min} are respectively the maximum and minimum value of the load factor, P_{Amax} = maximum breaking power at sea level, RPM = number of revolution per minute, Diameter = diameter of the propeller, h_{max} = maximum value of the propeller efficiency.

The characteristic parameters for the Cessna 182 can be found in Airliners.net (2015), Roud and Bruckert (2006) and McIver (2003). Some of the parameters, which were not readily available, were estimated from those of the very similar Cessna 172.

Table 7 Characteristic parameters of the Cessna 182

W_1 = 7,562 N	W_0 = 11,121 N	W_F =1737 N
b = 11.02 m	S = 16.1653 m^2	e = 0.75
C_{Lmax} = 2.10	C_{D0} = 0.029	n_{max} = 3.8, n_{min} = -1.52
P_{Amax} = 171.511 kW	RPM = 2,600	
Const. speed propeller	Diameter = 2.08 m	h_{max} = 0.80

A.2 Silver fox like UAV

The Silver Fox UAV is presently produced by Raytheon. Some specifications for the Silver Fox can be found at UAVGLOBAL Unmanned Systems and Manufacturers (2016). The power available $P_A(0)$ for the Silver Fox is only about 370 W, which allows it to climb only at low angles. Meanwhile, it is common for Radio Controlled (RC) airplanes to climb at very steep angles (See for example Granelli 2007). Thus, upon taking advantage of motors that have been developed in this domain, a Silver Fox-like airplane could be endowed with much more power in order to improve considerably its manoeuvre envelope. One such motor is the Zenoah GT-80 Twin

Cylinder 80cc (ZENE80T). It weighs 34 N and outputs 4045 W at 7500 rpm. (Horizon Hobby 2017). We shall consider a Silver Fox-like UAV with such a motor.

Table 8 Characteristic parameters of the Silver Fox-Like airplane.

$W_1 = 100.0$ N	$W_0 = 148.0$ N	$W_F = 19.1$ N
$b = 2.4$ m	$S = 0.768$ m^2	$e = 0.8$
$C_{Lmax} = 1.26$	$C_{D0} = 0.0251$	$n_{max} = 5.0$, $n_{min} = -2.0$
$P_{Amax} = 4.413$ kW	RPM = 7500	
Fixed pitch propeller	Diameter = 0.56 m	$h_{max} = 0.77$

A.3 Lockheed martin F-16

The General Dynamics/Lockheed Martin F-16 Fighting Falcon is a single-engine fighter aircraft originally developed for the United States Air Force. Its characteristic parameters can be found in Lockheed-Martin (2015), Filippone (2000) and Sadraey (2009). The maximum value of the lift coefficient and the maximum negative load factor were estimated from those of other similar fighter airplanes.

Table 9 Characteristic parameters of the F-16 fighter airplane

$W_1 = 90{,}237.4$ N	$W_0 = 213{,}365.6$ N	$V_{max} = 605$ m/s
$b = 10.0$ m	$S = 27.87$ m^2	$e = 0.8$
$C_{Lmax} = 1.8$	$C_{D0} = 0.026$	$n_{max} = 9.0$, $n_{min} = -3$
	$T_{Amax} = 131{,}222.5$ N	